4 Rethinking the Spectrum: The Digital (R)Evolution in Archaeological Aerial Reconnaissance

Geert J. Verhoeven

Introduction

Since Joseph Nicéphore Nièpce (1765–1833) invented 'drawing with light' in the 1820s, photography can almost celebrate its second centenary. Archaeological aerial photography covers approximately one half of that time span. The first aerial image was taken in 1858 from a tethered hot-air balloon by Gaspard-Félix Tournachon – also known as Nadar – of the village Petit Bicêtre (Colwell 1997; Newhall 1982). It was not, however, until June 1899 that the first (European) archaeological photograph (of the forum in Rome) was taken from a balloon by Giacomo Boni (Castrianni 2008). Despite the first flight of a manned, motor-driven machine built by Orville and Wilbur Wright in 1903, it was not until the end of World War I that archaeologically interesting pictures were made from an aeroplane. In this first phase of archaeological aerial reconnaissance, much credit must be given to Osbert Crawford (1886–1957). This Englishman is considered to be the inventor of scientific aerial reconnaissance and his work in the 1920s and beyond was the basis for the future development of aerial archaeology (e.g. Crawford 1924; 1929; 1933; Crawford and Keiller 1928).

Since Crawford and other pioneers of aerial archaeology such as Antoine Poidebard (1878–1955) and Theodor Wiegand (1864–1936), it has been known that archaeological remains can show up on the surface in a number of ways. Aside from standing structures (e.g. bridges, theatres, fortifications) and those partly eroded (e.g. earthen banks, mounds, ditches), most of the marks that can be viewed from above indicate buried archaeological remains. While the first type of archaeological feature is directly visible, the second type – often referred to as earthworks – is mostly recorded from the air when thrown into relief by low-angle sunlight (sometimes referred to as shadow marks), or in northern Europe by differential snow accumulations or differential melting of snow or frost (snow and frost marks). The buried or levelled remains may be revealed by visible tonal differences in the soil (soil marks) or differences in colour and/or height of vegetation above the buried remains (crop/vegetation marks), variations in the subsoil being mainly responsible for their creation. In other words, archaeological

remains must exhibit a localised contrast against the surrounding background in order to be detected (Beck 2007; Wilson 1982).

To date, the practise of archaeological aerial photography has been quite straightforward. In general, the images are acquired from the cabin of a low-flying aeroplane using a small- or medium-format hand-held photographic/still camera equipped with a lens that is commonly uncalibrated. Once airborne, the archaeologist flies around in a certain area, trying to detect possible archaeologically induced anomalies in the landscape. Once an anomaly is detected, it is captured in an oblique photograph and used for subsequent study. Although this specific type of data acquisition may seem strange to the non-archaeological community, the non-invasive approach yields easily interpretable imagery with abundant spatial detail, is extremely flexible and quite cost-efficient. Even though aerial archaeologists have been experimenting with different filters and film emulsions (Crawshaw 1995) and certain combinations sometimes rendered particular localised contrasts very well (e.g. near-infrared sensitised media with a yellow filter to image crop marks), the majority of archaeological aerial photographs have been shot using media that were sensitised only to visible radiation.

During the last decade, aerial archaeologists have started to use digital photographic cameras as their main working tool. Although the core functionality of still cameras has remained largely unaltered, the imaging sensors embedded in these digital devices are sensitive to both invisible Near-UltraViolet (NUV) and Near-InfraRed (NIR) radiation. This paper will therefore explore how these affordable, commercially available still cameras allow the acquisition of (narrowband) multispectral imagery in several visible and beyond-visible domains. In addition, the necessary theoretical underpinning will be provided in order to explain how and why the inherent spectral properties of current photographic cameras can be used to aid the detection and interpretation of archaeological anomalies.

Talking digital numbers

Archaeological aerial reconnaissance is just one part of the discipline called aerial archaeology. The latter encompasses the entire process from the acquisition and inventorying of imagery, to its mapping and final interpretation. It encompasses the study of all types of archaeological remains using data collected from an airborne platform: digital or film-based aerial photographs, airborne laser scanning, aerial imaging spectroscopy etc. As mentioned earlier, the majority of source data currently used by aerial archaeologists is acquired from the cabin of a low-flying aeroplane using still cameras. In the last decade, an increasing number of archaeologists have converted to a digital workflow, and digital photography is now commonplace in archaeological aerial reconnaissance. By acquiring the reflected visible portion of incident wavelengths radiated by the sun, digital photo cameras (from now on denoted DSCs or Digital

Still Cameras) taken aloft in aeroplanes allow the remote assessment of the vegetation status over both small and large areas. As their output renders archaeologically induced contrasts almost identically to the way the human visual system perceives them, DSCs have always been relied upon as aerial research instruments, without much consideration of the alternatives. However, applying DSCs as if they were film-based cameras does not help to advance the discipline of archaeological aerial reconnaissance. By outlining some basic operating principles of DSCs, it will be shown how scientists can exploit the spectral sensitivity of these devices to a far greater extent than is conventionally done, especially when these properties are related to the reflectance characteristics of the surfaces commonly imaged during an aerial survey (i.e. plants and soils).

Digital cameras

Aerial photography is a so-called passive remote sensing technique, because information about an object is gathered by capturing radiance originating from the object´s reflection of incident solar radiation. To acquire these data from the earth's surface by digital means, both an optical system and a dedicated sensor have to be used. Whether in a 'point-and-shoot' camera or a professional Digital Single-Lens Reflex (D-SLR), silicon is the basis for almost all digital image sensors in current DSCs. Without delving deeper into the physical background, this means that all conventional DSCs have a spectral sensitivity upper limit around 1100 nm (see Fig. 4.1), which is a wavelength that belongs to the Near-InfraRed spectral region (NIR; 700/750 nm to 1400 nm).

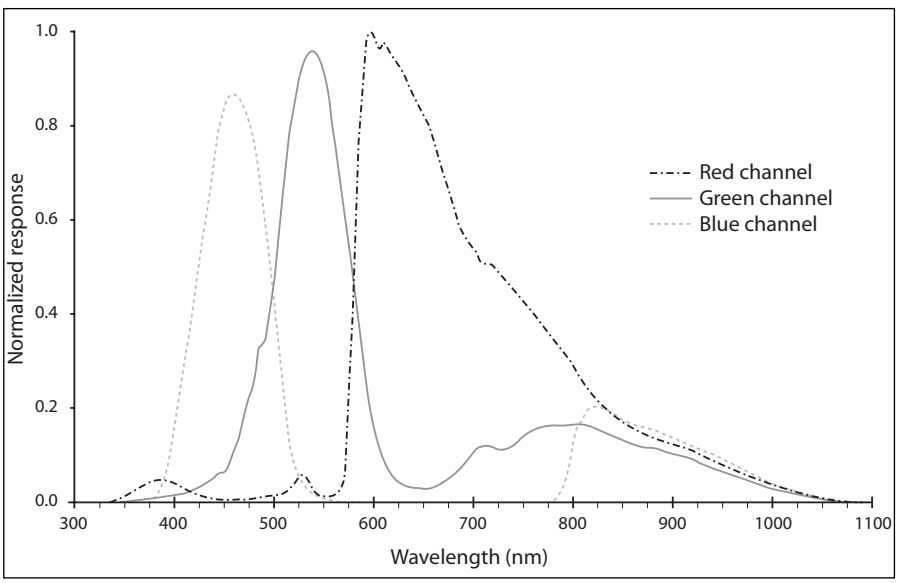

Figure 4.1: Spectral sensitivity of the Nikon D80 image sensor after removing the standard filter package (unpublished data by Philippe Smet – LumiLab, Ghent University – and Geert Verhoeven).

Conventional silicon imagers are also inherently sensitive to Near-UltraViolet radiation (NUV, also called UV-A or Long Wave UV; 315 nm to 400 nm), although to a far lesser extent then NIR (see Fig. 4.1). In general, the cut-off wavelength for off-the-shelf DSCs is around 330 nm to 370 nm (depending on the sensor). Because imaging of these invisible NUV and NIR wavelengths would be detrimental for image sharpness (all wavelengths have a different focus), exposure accuracy (DSC light meters are not calibrated for invisible radiation), and true colour reproduction, camera manufacturers place an NUV-NIR block filter (or hot mirror) on top of the sensor. As a result, the sensor's array of photosensitive detectors – called photodiodes – will generate a photographic signal by only taking the visible radiation into account (Fig. 4.2A).

Although such block filters come in various qualities (i.e. a number of DSCs retain considerable NUV and/or NIR response), their aim is equal: in so far as possible, preventing the invisible wavelengths from reaching the sensor. By removing this filter, the DSC becomes responsive to its full inherent spectral range (see Fig. 4.1). As noted above: the effect of such a modification is most noticeable when imaging the NIR waveband. Notwithstanding, the DSC's responsivity to NUV radiation also increases, although its sensitivity is far more modest in absolute terms (for an in-depth overview of sensor sensitivity and DSC modification, see Verhoeven 2008; Verhoeven and Schmitt 2010; Verhoeven *et al.* 2009b).

Although the imaging sensor is the heart of every digital camera, other components determine the final spectral response of a DSC. Whatever the type, all image sensors consist of a 2D-photodiode array to generate a digital photograph. However, photodiodes simply count photons; they are monochrome devices, unable to tell the difference between different wavelengths. Without further adaptation, they would only be able to create greyscale photographs. The most widespread way of providing colour sensitivity to a one-shot DSC image sensor is through the use of a Colour Filter Array (CFA). This mosaic pattern of coloured filters is positioned on top of the sensor (Fig. 4.2), allowing only particular spectral components of the incident radiation to

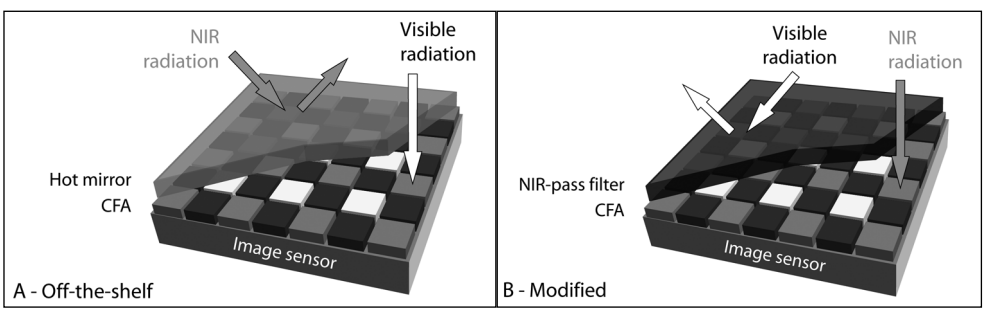

Figure 4.2: NIR-modification of a Bayer imaging array by replacing the hot mirror (Verhoeven 2008: fig. 10).

be collected (illustrated by Fig. 4.1). Almost all DSCs use a so-called Bayer pattern, a three-colour Red-Green-Blue (RGB) pattern in which the coloured filters are arranged as shown in Figure 4.2. A completely different approach was patented by Foveon Inc. This company created a particular kind of three-layered image sensor with a stack of three photodiodes at each sensor site, enabling the capture of all three R, G and B wavebands at the same location (Lyon and Hubel 2002). As this unique design is only implemented in very few DSCs, the remaining of this article will focus on the common Bayer CFA approach.

Image formats

Current one-shot DSCs generally offer different file formats to save the captured frames: JPEG, RAW, and/or TIFF. Although JPEG is the most commonly used file format world-wide, it is incapable of storing all originally captured data, something that is also true to a certain extent for big TIFF files. Therefore, most professional photographers prefer shooting RAW. In essence, a RAW file is nothing but an array of digital numbers, each of them generated by one photodiode and proportional to the incoming radiation of a certain wavelength range (determined by the coloured filter on top) plus some offset due to dark current and bias. It is essential to understand that a RAW file has not been subjected to any major colour-processing algorithm by the camera's embedded software, unlike in-camera generated JPEGs and TIFFs. Consequently, a RAW file has to be developed with a dedicated RAW converter in the computer in order to yield a normal-looking image. However, it also means that a RAW file embeds the most 'pristine' data generated by the DSC. As it is very important to work with these initially generated integer values, using a RAW-workflow is crucial in any scientific (aerial) photography (Verhoeven 2010).

Revealing stress

Of all possible contrasts, those manifested as crop or vegetation marks are the most abundant and generally provide many details of the subsurface archaeology. Hence, this contribution mainly focuses on new imaging techniques beneficial for the detection of (faint) archaeologically induced crop marks. Because the spectral properties of DSCs have to be related to the imaging of crop marks, it is instructive to start with a basic knowledge of a plant's reflectance properties. Firstly, a basic overview of the spectral responses (and their information content) from individual leaves will be provided, after which this knowledge will be transferred to the canopy level. As the sensors of DSCs are responsive to radiant energy from about 330 nm to 1100 nm, only the spectral properties of vegetation in the NUV (315 nm to 400 nm), visible (400 nm to 700/750 nm) and NIR (700/750 nm to 1400 nm) spectral domains are of concern.

Individual leaves

When trying to detect stress in plants, it is important to understand the fundamental spectral reflectance characteristics of green leaves illustrated in Figure 4.3. In particular, this illustration displays the reflectance curve of a healthy green radiata pine leaf together with the spectral reflection of the same leaf when suffering from nitrogen (N) deficiency. Current knowledge allows us to distinguish the following commonly accepted spectral leaf reflectance and absorption features for all green plants in the NUV, visible and NIR domain (Buschmann and Nagel 1993; Caldwell 1971; Carter 1993; 1994; Carter and Estep 2002; Carter and Knapp 2001; Chappelle *et al.* 1992; Gitelson and Merzlyak 1994a; 1994b; 1996; Gitelson *et al.* 1996; 2003; Grant *et al.* 2003; Hatfield *et al.* 2008).

Near-UltraViolet (NUV; 315 nm to 400 nm)

Concerning the NUV part of the electromagnetic spectrum, it remains difficult to present many figures on particular spectral properties of vegetation species because studies on NUV absorption and reflectance of natural and artificial surfaces are still largely lacking in the field of terrestrial remote sensing. In general, the spectral signatures are less distinct in the NUV when compared to the NIR or visual domain, for both

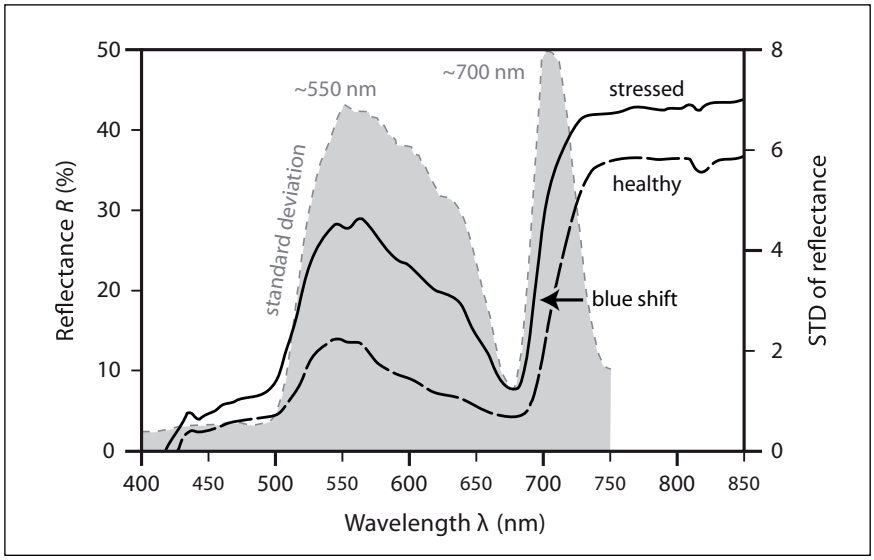

Figure 4.3: Typical reflectance responses of a radiata pine leaf. The discontinuous curve represents the mean reflectance for healthy, chlorophyll-rich leaves, while the upper curve indicates the mean reflectance for a stress situation (nitrogen deficiency). The grey curve represents the standard deviation of reflectance calculated from reflectance spectra of maize leaves with varying chlorophyll content (adapted from Carter and Estep 2002: fig. 2B, and Hatfield et al. *2008: fig. 2 respectively).*

dissimilar types of vegetation and different states of plant vigour. Most plants reflect very small amounts of NUV (around 5%) while the majority is absorbed. Accordingly, one might conclude that NUV imaging will not be particularly suited for detecting stress marks in plants. However, it is worth trying to generate NUV photographs of stressed vegetation, as it has not previously been done for archaeological purposes.

Visible (400 nm to 700/750 nm)

The previous situation contrasts sharply with the visible reflectance as the latter has been very well studied the last decades. Besides its crucial role in a plant's oxygen production, it is well-established that the presence of leaf chlorophyll, a green pigment which comes in both a Chlorophyll a (Chl a) and a Chlorophyll b (Chl b) variant, largely dictates how plants appear spectrally in the visible domain. Moreover, chlorophyll content is strongly related to plant senescence and stress. Consequently, both spectral curves do not only give major clues to the amount of this photosynthetic pigment in a plant's leaf, but also indicate the plant's health status. Generally speaking, visible leaf reflectance decreases with increasing chlorophyll content. When the chlorophyll content decreases due to plant stress or seasonal senescence, the total leaf reflectance increases. This behaviour is the most consistent leaf response to plant stress within the 400 nm to 2500 nm spectrum. Furthermore:

- the Blue band (400 nm to 500 nm) is more or less insensitive to variations in the pigment content due to the fact that Chl a and Chl b pigments absorb strongly in this range, while also other important plant pigments have a high absorption coefficient in this region;
- near 670 nm (i.e. in the Red band of 600 nm to 700/750 nm), the reflectance and absorption only change in relation to chlorophyll content when its amount is very low to moderate. Once a leaf exceeds 100 mg/m^2 chlorophyll, the total absorption remains unaltered;
- the highest sensitivity of the reflectance curve to chlorophyll pigment variation occurs in the Green spectrum around 550 nm and in the Red Edge (i.e. the steep slope of the reflectance curve around 700 nm in the far-Red to NIR transition spectrum – see Fig. 4.3), because the absorption of Chl a and Chl b is very low in these regions. As a result, even very small changes in pigment content can alter the reflectance. This observation is confirmed by the grey curve in Figure 4.3, which represents the standard deviation of reflectance calculated from several spectra of maize leaves containing different chlorophyll concentrations. Besides confirming the statement about the Blue waveband, this curve clearly illustrates the dispersion of reflectance data to be largest in the 530 nm to 590 nm zone and around 700 nm. This sensitivity results in two very generic stress responses: the Green reflectance peak around 550 nm is broadened towards longer wavelengths and causes the leaf to appear yellowish (a phenomenon called chlorosis). At the same time, the Red Edge

shifts toward shorter wavelengths due to the stress related increase of reflectance at wavelengths near 700 nm (Fig. 4.3). This Blue shift of the Red Edge is currently accepted as the most consistent stress response of plants to different stressors. Hence, it is the second region of interest in this study.

Near-InfraRed (NIR; 700/750 nm to 1400 nm)

In the NIR region, the spectral properties of leaves are no longer governed by pigments. As a matter of fact, heavy scattering takes place inside the leaf's internal cellular structure –in particular the spongy parenchyma mesophyll. The very steep increase in reflectance of electromagnetic energy between 700 nm and 750 nm is the aforementioned Red Edge: the most prominent characteristic in the reflectance spectrum of healthy vegetation. This transition zone of very abrupt reflectance change results from the fact that the absorption by chlorophyll pigments is low and the NIR reflection by the spongy mesophyll increases, giving rise to one of the most extreme slopes to be found in reflectance spectra of natural materials. Figure 4.3 shows that healthy green leaves often respond to short-term, acute stressors with a slight increase in NIR reflectance. This certainly holds when plants suffer from dehydration. In most books on remote sensing, it is suggested that the plant's NIR reflectance significantly decreases when a plant is stressed. However, this will only occur in cases of chronic water shortage or disease, end-of-season senescence, or heavily nutrient-deficient vegetation (all corresponding to the effect of major internal tissue degradation). At this stage, also the Red Edge disappears completely. Because of this variation in NIR reflectance, imaging crops in this spectral range will be the third study domain.

Canopy

Reflectance from the canopy might differ significantly from that of an individual leaf, because canopy reflectance combines soil background reflectance, shadows, reflectance from weeds and non-green canopy components as well as the anisotropic behaviour of the canopy and its varying architecture (Guyot 1990; Myneni *et al.* 1995). As a result, the information transfer from a leaf's reflectance to the reflectance of the canopy is often nonlinear, while leaf-based reflectance spectra might not directly and as a whole be transferable to the canopy level. Canopies with a high LAI (i.e. Leaf Area Index or leaf area per unit of ground) can be characterised by a significant increase in NIR reflectance due to the process of leaf additive reflectance, while the reflectance from the ground might also increase the total reflectance in the Red band when imaging early in the growing season. In general, the spectral contribution of the soil is negligible if the canopy consists of a large number of healthy, mature leaf layers (Guyot 1990; Myers *et al.* 1970). Gitelson *et al.* (2002) have shown that the spectral features of wheat canopy reflectance closely resemble those of individual leaves when the Vegetation Fraction (VF) reaches 60%.

Even though several techniques exist to counteract such particular canopy issues, many approaches currently used for canopy remote sensing were specifically developed

on the basis of individual leaf reflectance and most have proved to yield decent results. Moreover, archaeological reconnaissance does not require accurately estimating particular crop parameters like the exact amount of chlorophyll. What matters are reliable, generally applicable methods that can be extended across entire landscapes, at different times of the day, and during various growing seasons, rather than very specific approaches that might vary from field to field, crop to crop, and by time of year. These remote sensing methods should allow us to image the contrast exhibited (directly or indirectly) by an archaeological residue in its surrounding matrix, without the need to optimise the approach on the basis of crop species. Finally, the imagery resulting from aerial archaeological reconnaissance commonly has a large spatial resolution, which means that it almost always operates at the leaf level. For all these reasons, the methods presented here are very straightforward and all deduced from the spectral characteristics of leaves.

Putting everything together

As outlined above, the NUV, Red Edge and NIR regions will be focused on. All three spectral zones are discussed in the following sections. Besides mentioning the necessary hardware components needed, an overview of some photographic results will be given. As imaging the NIR radiance is by far the easiest of all three approaches, the order of the following overview is not determined by increasing wavelength, but by increasing imaging complexity.

NIR

Since Sir Frederick William Herschel (1738–1822) discovered the InfraRed (IR) portion of the electromagnetic spectrum in 1800, many scientific disciplines have become fascinated by this kind of invisible radiation. Interest increased after World War II, as colour infrared emulsions had shown their capabilities. Despite its large potential in aerial reconnaissance, very little, mostly unsystematic effort has been made to incorporate NIR radiation in archaeological work by means of Black-and-White (B&W) and False Colour InfraRed film (FCIR or more commonly CIR). This phenomenon can largely be attributed to the error-prone film-based workflow of pure NIR or CIR imaging, some unfamiliarity with its principles and the fact that such a beyond-visible approach did not always prove successful or even useful. Thorough assessment of the full archaeological potential has also been problematic due to the general lack of simultaneously acquired and geographically extended comparative material from the visible spectrum (Verhoeven 2008; 2009; 2011). Because aerial photography in the NIR spectral range is by far the easiest of all spectral domains that are discussed here, this section will present the most detailed exploration.

Material

Most of the presented NIR imagery was captured with a modified Nikon D50 (hereafter called $D50_{NIR}$), whose spectral response curves are shown in Figure 4.4A. This response was yielded by inserting a NUV+visible blocking filter in front of the sensor (see Figure 4.2B). In a second phase, a Full Spectrum-modified Nikon D80 was taken aloft (denoted $D80_{FS}$ – see Fig. 4.1), as it generates digital frames with a higher pixel count and accepts larger memory cards. To acquire pure NIR images with the latter camera, its lens was equipped with a Hoya R72 filter. Simultaneous visible and NIR data acquisition was allowed by a custom-built camera rig on which both a modified Nikon and an unmodified Nikon D200 were mounted. Each of them was fitted with an identical AF Nikkor 50 mm f/1.8D lens whose focus was fixed on infinity (for more details on lenses and filters that can be used, consider Verhoeven 2008; 2009; 2011). As is conventionally done in archaeological reconnaissance, a small GPS receiver always logged the complete flight path to enable easy georeferencing of the images. Taking out the door of the aircraft ensured a maximised field of view and enabled easier handling of the cameras inside such a small aircraft (Fig. 4.4B). This approach was used for all subsequently presented aerial images, which were acquired in the central Italian Regione Marche.

To make sure that only pure NIR imagery was used for the following comparison, the Blue channels were extracted from the $D50_{NIR}$ and $D80_{FS}$ imagery. To compare the two data sets by objective means, both the visible and pure NIR frames were subjected to histogram stretching to optimise the images' global contrast.

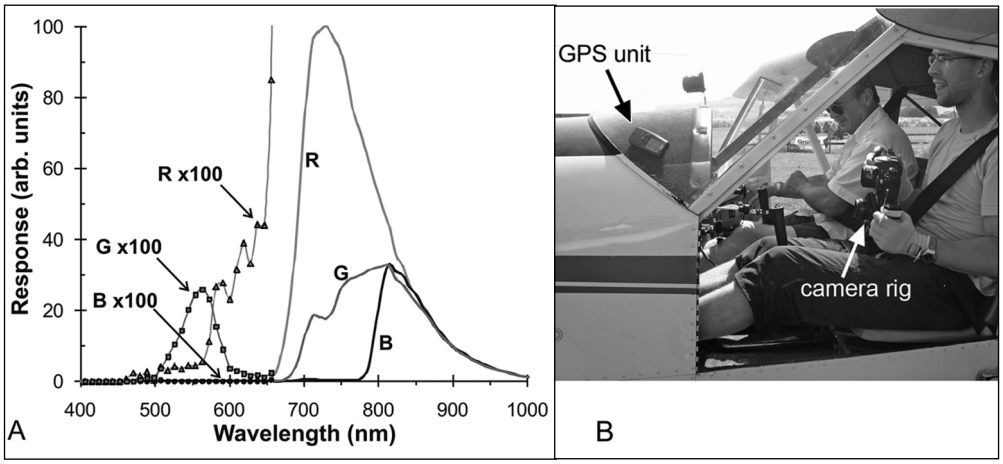

Figure 4.4. (A) Relative response versus wavelength of the Nikon $D50_{NIR}$ with a Nikkor 20 mm f/3.5 AI-S (Verhoeven et al. 2009b: fig. 5); (B) inside a two-seater aeroplane (Cessna 172) holding a two-DSC rig (photograph by F. Vermeulen – Ghent University).

Results

Figure 4.5 depicts the central part of the Roman coastal colony of Potentia. The aerial frames were shot in the middle of May 2008 and clearly confirm that chlorotic vegetation is very difficult to distinguish in the NIR (compare visible frame 4.5A with NIR frame 4.5B). When this stress-related loss of chlorophyll pigment is rather moderate, the yellow discolouration of vegetation is not extremely pronounced, but the alteration of the NIR reflectance curve can even be smaller. Pushing the local contrast in both frames (Fig. 4.5A and 4.5B) to the limits (Fig. 4.5C and 4.5D) does not alter this observation: even though the resulting tonal differences clearly prove the spectral NIR responses of chlorotic and healthy green vegetation to be dissimilar (Fig. 4.5D), the number of features perceptible as well as the distinctness of the archaeological traces still remain superior in the visible spectrum.

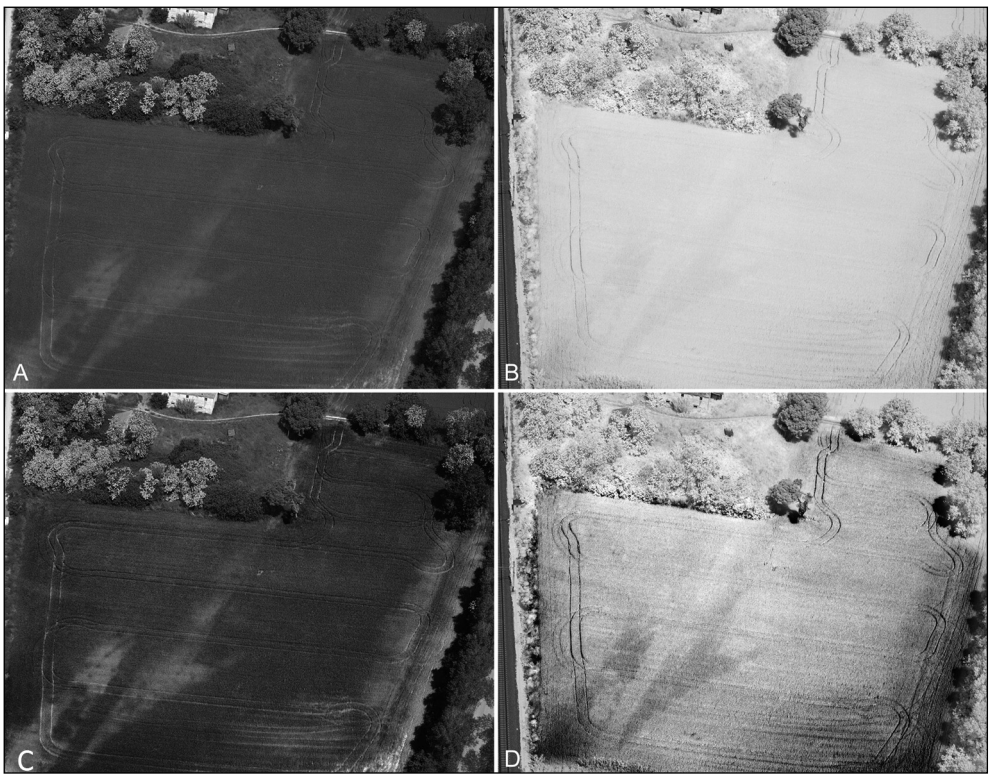

Figure 4.5. (A) Visible image of the central part of the Roman town of Potentia (N 43° 24' 53", E 13° 40' 14" – WGS84); (B) NIR image of the same scene. To obtain versions (C) and (D), very extreme local contrast enhancement was applied to (A) and (B) respectively. Images acquired with a Nikon D200 (A) and a Nikon D50$_{NIR}$ (B) on May 15, 2008 at 11.14 h (Verhoeven 2009: fig. 9.6).

On the other hand, pure NIR channels can clearly reveal the more severe drought and nutrient stress in the canopy reflectance. Imagery taken during the hot summer of 2008, again above the Roman city of Potentia, clearly illustrates this. In the cereal field on the right side of Figure 4.6A, small pieces of the street network in the southern part of the city are visible. The NIR record (Fig. 4.6B), however, allows many more traces to be seen, while the features are also more distinct when compared to the visible record. Because it is ripe, the overall visible reflectance response of the cereal crop is higher and the human visual system perceives these crops as yellow-brown. Therefore, the reflectance increase of grain growing over a rocky sub-surface can only be slightly

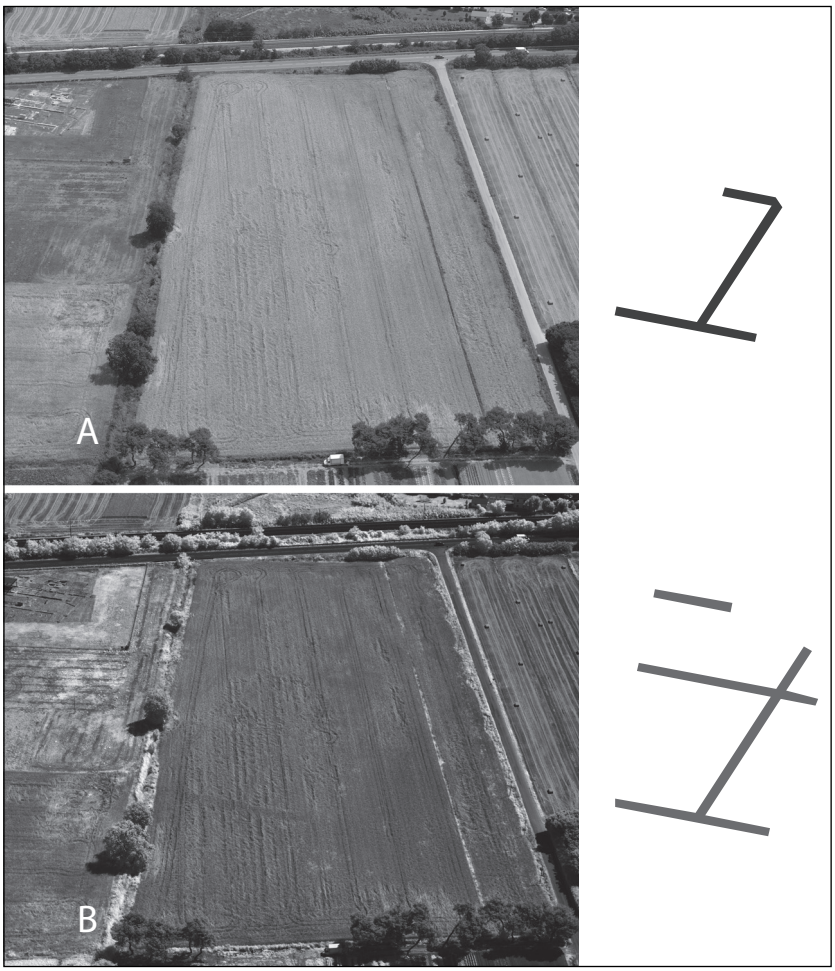

Figure 4.6: A) Visible image of the southern part of Potentia, while (B) displays the same view in the NIR. The imagery was acquired with a Nikon D200 (A) and a Nikon D80$_{FS}$ (B) on July 03, 2008 at 11.02 h (Verhoeven 2009: fig. 9.7).

larger in comparison with the adjacent crops. In the NIR, the global reflectance decreases seriously at this stage of the crop cycle, but Figure 4.6B proves the total reduction of NIR reflectance to be noticeably larger for the extremely stressed plants. After additional contrast enhancement had been performed, the traces that could be mapped in the cereal field were indicated on the right of Figure 4.6A and Figure 4.6B. These results nicely confirm the statements made previously by Hampton (1974), who also empirically attested NIR imaging to be superior for cereal crop mark imaging late in the season. For more examples of NIR negative crop marks as well as positive crop marks (i.e. features that are characterised by a larger vegetation biomass and, as a consequence, will reflect more NIR radiant energy), the reader should consult Verhoeven 2009 and 2011.

Although the above examples clearly indicate the spectral response in the NIR to be unrelated to chlorophyll pigment concentration, the most striking example is given in Figure 4.7, which presents two different photographs of the central part of the Roman town Trea. Figure 4.7A again depicts the visible bands, together with the $D50_{NIR}$ image (Fig. 4.7B). Whereas the visible image only shows strange, non-archaeological positive vegetation marks (perhaps due to differential manuring or a dissimilar kind of crop), the NIR image clearly reveals the outlines of a Roman temple. Besides the masking effect of the chlorophyll pigment, this striking difference might also be attributed to the anisotropic behaviour of the vegetation canopy. Being a non-Lambertian surface, the reflectance of the vegetation canopy is not equal in all directions, but is dependent upon the sun and sensor zenith/off-nadir and azimuth angle (the phenomenon of

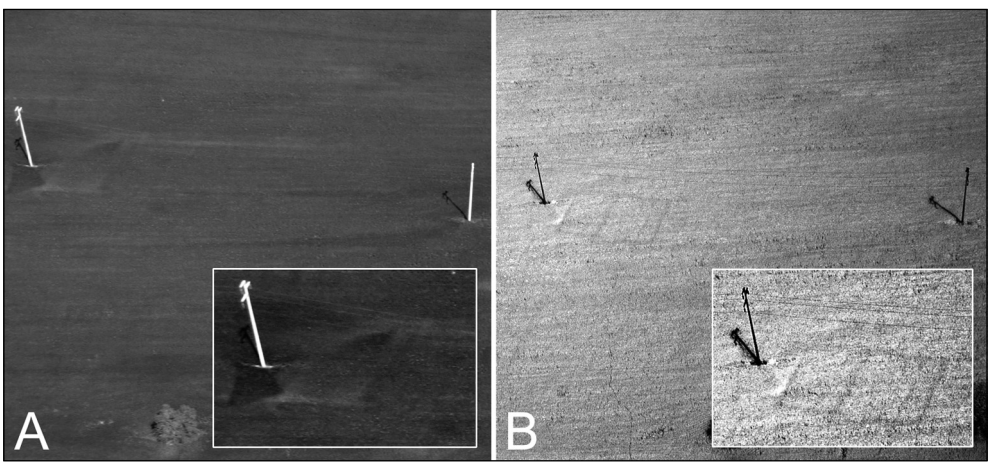

Figure 4.7: A visible (A) and pure NIR image (B) of Roman Trea's central part (N 43° 18' 40", E 13° 18' 42" – WGS84). The insets are high contrast enlargements of the same area around the left pylon. Images acquired with a Canon EOS 300D (A) and a Nikon $D50_{NIR}$ (B) on April 23, 2007 at 11.01 h (Verhoeven 2009: fig. 9.10).

crop marks being clearly visible from one specific direction of view is widely known among aerial archaeologists). This reflectance anisotropy reaches a maximum at visible wavelengths, whereas NIR radiation is relatively free of such bidirectional effects due to the multiple canopy scattering of NIR photons. Concerning this, the less critical angular view that is characteristic for the NIR approach might prove very useful, certainly in cases where one would opt to fly a complete vertical coverage and try to detect archaeological features afterwards.

Red Edge

Based on the theoretical spectral reflectance facts outlined before, it seemed archaeologically very interesting to detect the generic stress related Blue shift of the Red Edge by performing a ratio analysis of reflectance spectra (R), more in particular R_{700}/R_{800}. This index can be denoted a spectral pigment index because it employs ratios of narrow spectral bands that are respectively sensitive and insensitive to pigment content (Blackburn 2006). R_{800} is used as a denominator to standardise the Red Edge reflectance.

Material

As two very narrow spectral bands are needed and a visual image is necessary for reasons of comparison, three DSCs were fitted to a single bar, allowing for simultaneous data acquisition. The visual comparison frames were generated with a Nikon D200 plus AF-S Nikkor 18–70 mm f/3.5–4.5G ED lens (fixed on the infinity setting at 50 mm), while the Nikon $D80_{FS}$ and Nikon $D50_{NIR}$ allowed to capture beyond visible data. On the one hand, the Nikon $D50_{NIR}$ plus an AF Nikkor 50 mm f/1.8D registered pure NIR radiance. The 800 nm band was provided by extracting the Blue channel from these raw $D50_{NIR}$ data. On the other, the $D80_{FS}$ was fitted with an identical lens and a Carl Zeiss interference filter. Since this filter has its central wavelength λ_c at 702 nm and a spectral transmission (quoted in terms of the 50% transmission points) from 696 nm to 708 nm, this DSC-lens-filter combination made it possible to acquire Red Edge radiance data. Radio controlled triggers allowed the DSCs to operate simultaneously (consult Verhoeven 2009 for details).

Results

Figure 4.8 shows the generation of this simple vegetation index on the central part of the Roman city of Trea. Figures 4.8A, 4.8B and 4.8C are JPEG-compressed frames as they would have been created by the Nikon D200, Nikon $D80_{FS}$, and Nikon $D50_{NIR}$ respectively. The second row illustrates the results of the first two processing steps: all three frames are co-registered and the Red (E) channel extracted from the 700 nm frame, while the Blue channel (F) is extracted from the NIR frame (C). As explained, these operations are performed on the RAW data.

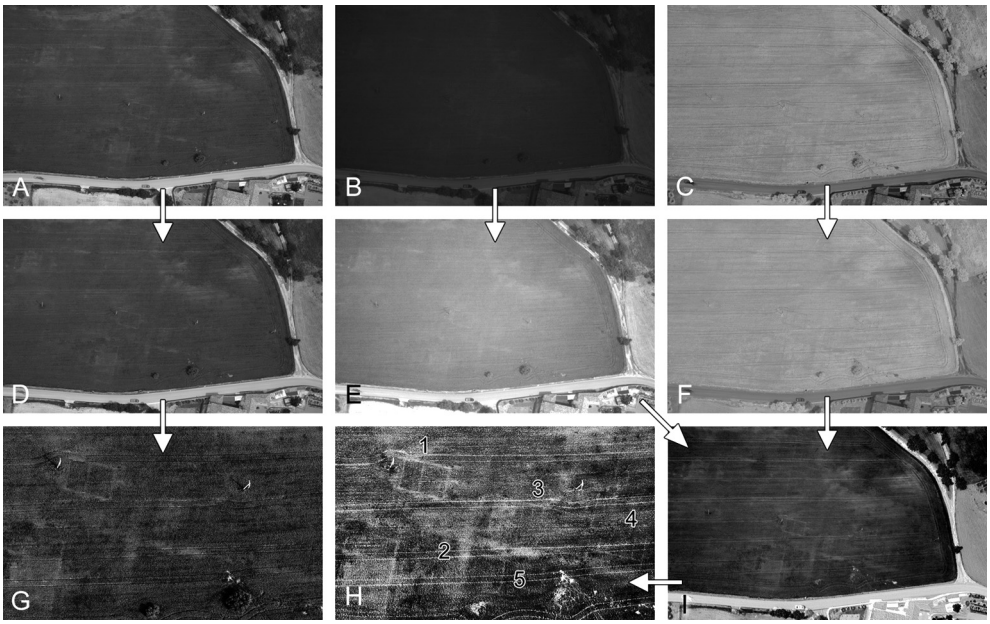

Figure 4.8: Creation of the reflectance ratio image (tile I and H) and comparison with a simultaneously generated conventional colour photograph (G). By revealing previously invisible building structures in the central part of the Roman city of Trea, tile H indicates the revealing power of the R_{700}/R_{800} index. The imagery was acquired with a Nikon D200 (A), a Nikon $D80_{FS}$ (B) and a Nikon $D50_{NIR}$ (C) on May 15, 2008 at 11.38 h (Verhoeven 2009: fig. 11.5).

At this stage, image Figure 4.8E represents the 700 nm data (i.e. the numerator of the VI), while Figure 4.8F shows the 800 nm record (i.e. the denominator of the VI). Dividing both images yields Figure 4.8I. This output, which was visualised with a linear 2% stretch of the data, represents the R_{700}/R_{800} index, which clearly indicates chlorophyll-rich zones to be darker than non-vegetated zones (i.e. the ratio increases as leaf chlorophyll content decreases). To compare this reflectance ratio image with the conventional colour image, the local contrast of both frames Figure 4.8A and Figure 4.8I was seriously enhanced and their central portion represented in Figures 4.8G and 4.8H respectively. This combination clearly shows the vegetation index to yield more archaeologically relevant data: whereas the large structures such as the Roman temple (1) and roads (2) are apparent in both frames, much smaller features – most likely representing walls of tabernae (3, 4, 5) – are only displayed in the R_{700}/R_{800} output. This indicates that the stress-induced response in the plants overgrowing them was still too weak at the time of acquisition to be detected by common aerial imagery. The VI, however, maximally exploited the dissimilar reflectance properties in the two narrow spectral bands.

NUV

Compared with visible and NIR aerial photography, reflected NUV airborne imaging is quite problematic. Besides the very modest portions of terrestrial NUV, this radiation is seriously subjected to Rayleigh scattering, a physical process that alters the trajectory of the incident sun radiation and causes a lot of diffuse terrestrial NUV. From a remote sensing point of view, such a situation is detrimental, because this diffuse component (perceived as haze in the visible domain) causes a reduction in visibility, a diminution of contrast and thus also a loss of detail (Rees 2001). As this masking effect increases with increasing flying height, NUV aerial imaging can only be successfully performed from low altitudes (Cronin *et al.* 1968). Thirdly, the NUV reflectance of most objects is very low: 5% to 10% (Gruzdev *et al.* 2003). Obviously, NUV aerial remote sensing is only applied in a few, very specific applications: e.g. detecting oil spills on water and dry land using passive or active systems (e.g. Vizy 1974). For these reasons, aerial NUV photography has never been used in archaeological research (as far as the author is aware of), although Gibson (1978) states that it might be useful in revealing soil marks, but no further reference or illustrative material proves this point.

Material

To decently image NUV, one not only needs a modified digital camera (here fulfilled by the aforementioned Nikon $D80_{FS}$ – Fig. 4.1), but also a very specific filter and lens. Equipping a DSC with a NUV capable lens is less straightforward than might be expected. In general, optical glass does not transmit much NUV and becomes completely opaque to electromagnetic radiation below 350 nm, while optical cements and lens coatings might additionally decrease the NUV transmittance (Ray 2002). As a result, most photographic lenses are unsuitable for NUV imaging (see the Zeiss Topar transmission curve in Figure 4.9). However, expensive expert lenses with special quartz and fluorite elements for sub-350 nm imaging do exist (see Verhoeven and Schmitt 2010 for an overview). Unfortunately, none of these exist in wide-angle variants. Fortunately, some older lenses still have a useful NUV transmission below 350 nm due to their simple optical design with few lens elements and the absence of cemented or multi-coated elements (Rørslett 2004.). The discontinued Novoflex Noflexar 35 mm f/3.5 is such a lens, characterised by a cut-on transmitted wavelength of about 330 nm (Fig. 4.9) and used in the acquisition of all following images.

Thirdly, a Baader Planetarium U-Filter (also called Venus Filter) is mounted onto the lens. This interference filter is a very important part of the complete imaging system, because the NIR response of a D-SLR hugely increases when removing the internal cut-off filter. As most NUV pass filters seriously leak in the NIR domain (see the transmission curve of the Hoya U-340 filter in Fig. 4.9), they are unsuited for pure NUV imaging. The Baader filter on the other hand is a very dense visual+NIR blocking, NUV transmissive filter (Fig. 4.9). Without it, the final digital frame would still be heavily NIR contaminated, rendering the resulting images useless.

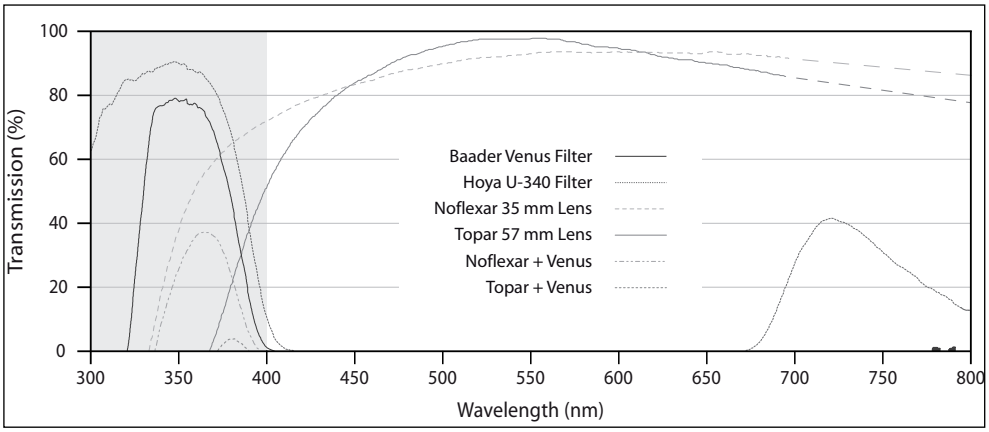

Figure 4.9: Spectral transmission of several mentioned optical elements (Verhoeven and Schmitt 2010: fig. 8).

Because even a converted D-SLR is only moderately sensitive to NUV and the optics as well as the interference filter absorb NUV to some extent, imaging the very small quantities of reflected NUV makes long shutters speeds inevitable. To tackle this issue, a radio-controlled platform – built around a Helikite – was used as an appropriate, stable and low-flying aerial platform (Verhoeven *et al.* 2009a).

Results

In accordance with the theory, none of the NUV photographs shot so far could visualise vegetation marks better than a normal colour image. On those locations where NUV crop marks showed up, it seemed that they were mainly visible due to a scarcely vegetated surface, rather than a stress induced discolouration of the grass (Verhoeven and Schmitt 2010). Even though the crop mark related NUV 'evidence' collected so far is extremely limited, this already gives some clues to the uselessness of imaging with these shorter-than-visible-wavelengths to reveal vegetation marks.

However, the first set of NUV images clearly showed that NUV imaging might have significant potential for imaging sediment differences in soil. Figure 4.10 indicates the contrast difference between the white gravel and the surrounding matrix to be more pronounced in the processed NUV frame (Fig. 4.10C) compared to the visual image (Fig. 4.10A). Again, the interpretation of this result is to some extent limited by the existing reflectance studies. In addition, the reflectance of soil is far more complex than vegetation, because it is not an ideal system and the link between particular soil attributes and measured soil chemistry is complex. However, research by Doda and Green (1980; 1981), clearly showed that the NUV reflectance of dissimilar sands can be very different. A possible explanation for these dissimilarities can be found in their different particle size, which is known to be of main influence on the reflectance of

Figure 4.10 Comparison between a visible frame (A), unprocessed RAW NUV image (B) and enhanced NUV photograph (C) of an excavation area in Potentia. The large dark blob in the upper right corner of (B) and (C) is the shadow cast by the Helikite. The images were acquired with a Nikon D70s on July 05, 2008 at 12.06 h (A) and a Nikon D80$_{FS}$ at 13.59 h on the same day (B–C) (Verhoeven and Schmitt 2010: fig. 12).

soils. This is not only applicable to the NUV: in almost the whole of the 225 nm to 2550 nm band, the reflection of sandy soils is highest for fine particles, with the greatest absorption for coarse soils, but the absorption difference between coarse and fine soils is slightly greater in the NUV and Blue compared to the remaining of the visible range (Doda and Green 1980; 1981). Furthermore, Cronin *et al.* (1968) reported that the reflectance difference between rock with rounded and angular grains was greatest in the NUV, while Dorwin (1967) and Glässer *et al.* (1989) proved the usefulness of terrestrial NUV photography in a geological and archaeological context respectively. It therefore seems reasonable to conclude that soil mark visualisation can in certain cases benefit from an aerial archaeological NUV approach.

A comparison of the visual image (Fig. 4.10A) with the processed NUV frame (Fig. 4.10C) also indicates the abundant spatial details visible in the latter, although the normal colour photograph was shot with a superior lens and a much higher shutter speed. This reveals the potential higher spatial resolution of an NUV image, to be attributed to the shorter wavelengths used for imaging.

These results thus indicate that aerial NUV photography – although not as straightforward as other forms of optical imaging – might be beneficial for archaeological soil related research. However, far more evidence is needed (both in terms of spectral curves and imagery) before the real benefits of archaeological NUV imaging can be accurately outlined and quantified.

Conclusions

In archaeological aerial reconnaissance, analogue cameras have been used for almost a century. In the last decade, straight-out-of-the-box Digital Still Cameras (DSCs) have also become a standard tool for the aerial archaeologists. However, using DSCs in the

same way as analogue film-based cameras were used, will not really help in advancing the discipline of archaeological aerial reconnaissance. Even though various air- and space-borne remote sensing systems have the capacity to offer new imagery acquired in very small to very broad wavebands (both visible and invisible), few of them (if any) generate images in the same flexible and economical way as active aerial photography from a low-flying aeroplane does. Therefore, means must be found to maximise the information gathered by the common latter approach, both during the image acquisition phase and afterwards during the processing of the generated data.

Given this, it is striking that more than a century after aerial archaeology was initiated, the basic routines of active aerial reconnaissance are still largely identical to those of the true pioneers. The methods and techniques of aerial imaging in the Near-UltraViolet (NUV) waveband, the Red Edge zone, and the Near-InfraRed (NIR) spectral region are some of the author's attempts to tackle this issue. Moreover, it has been proven that these data can be generated using the same tools aerial archaeologists normally use: digital small-format photographic cameras.

Although archaeological NIR aerial imaging is by no means novel and has been performed before in the analogue era, the advantages that modified DSCs can offer in terms of the generation and interpretation of reconnaissance data are substantial, using individual pure NIR spectral channels on the one hand and arithmetic operations performed on a combination of channels on the other. When combined with information from the visible wavebands (400 nm to 700 nm) and radiance data from the Red Edge spectral region, many new opportunities are provided to visually enhance archaeologically related anomalies (more specifically crop marks) and/or even reveal completely new features. In addition to simplifying the complete workflow, the modified DSCs thus seriously expand and perfect some of the possibilities known from the film-based approaches, without the significant costs and workflow-related drawbacks of the latter. Data acquisition in a more energetic part of the electromagnetic spectrum (i.e. the NUV) has proven to be more difficult. However, the real-world examples provided have shown that NUV photography could be really beneficial for soil mark archaeology once most of the practical problems are solved.

Despite these interesting results, some existing drawbacks still need to be resolved before this research can be really beneficial for the broader archaeological community.

- More spectral reflectance data are needed, specifically collected above archaeological visibility marks (i.e. mainly crop and soil marks). All terrestrial objects have very specific spectral reflection, transmission, absorption, and emission characteristics. In order to exploit these objects' spectral signatures, it is of the utmost importance to understand how and why particular objects reflect incoming solar radiation. Only when these characteristics are understood, can new targeted imaging approaches and processing techniques be presented.

- There is currently a lack of new procedures to extract information from digital colour frames generated by taking only the reflected portion of the visible light into account. Certainly when one knows that these photographs make up a very large portion of all archaeological reconnaissance data ever generated, building new methods to analyse them might be seen as the most important new approach which we await.
- Fast and accurate georeferencing procedures are desperately required. Irrespective of the method applied, current approaches are too time-consuming. Especially in large-scale archaeological projects with thousands of images, this georeferencing step is currently considered one of the biggest bottlenecks. Additionally, also specialised software, reference data, photogrammetric skills and experience might be required. Consequently, aerial archaeology does often not go beyond the data acquisition stage. Since many aerial photographs never get accurately georeferenced, their potential is barely exploited. Therefore, automated georeferencing techniques are highly desirable (Verhoeven *et al.* 2012).
- Finally, there is the major drawback of the reconnaissance method itself. No matter how efficient and accurate these new tools can be, an increase in site discovery rate using multispectral imaging with DSCs is unlikely as long as the predominant flying strategy of 'observer-directed' survey (i.e. only features spotted from the aeroplane will be photographed) is practised. This approach generates extremely biased data that are totally dependent on an airborne observer recognising archaeological phenomena (Palmer 2007). Thus, subsurface soil disturbances that are visually imperceptible at the time of flying will not make it into a photograph, even if their particular spectral response in a particular waveband might exhibit enough contrast with the surrounding matrix.
- In an attempt to address these shortcomings, there is a need to formulate some guidelines and future research topics. In essence, such future research needs to improve the validity of all presented methodological-technological innovations and make them easily accessible for interested parties. In essence, this is what the newly-founded Ludwig Boltzmann Institute for Archaeological Prospection and Virtual Archaeology will focus upon (besides many other things). This Vienna-based research institute consists of three main programme lines: Archaeological Remote Sensing, Archaeological Geophysical Prospection, and Archaeological Interpretation, Spatial Analysis and Virtual Archaeology (Doneus and Neubauer 2010). In the first programme line, the LBI wants to further develop efficient archaeological prospection techniques in the fields of Airborne Laser Scanning (ALS), Airborne Hyperspectral Scanning (AHS) and conventional archaeological reconnaissance. Besides focusing on the fast and accurate auto-georeferencing of newly (and previously) shot aerial images, one of the general aims is to broaden the current understanding of the spectral properties of vegetation and soils. By collecting spectral data above places with known buried archaeology and so-called sterile places on a weekly basis, it is hoped to get more insight into the formation

of spectral contrast throughout the growing season of a plant and different stages of soil management. These data will indicate which spectral bands should be used to maximise the local contrast looked for, besides revealing the best periods to get airborne. This information is not only suited to analyse the high resolution, strip-wise flown hyperspectral data sets that the LBI acquires, but it will also aid in the building of low-cost imaging tools that can be taken aloft by anybody. It thus seems self-evident that the currently sketched out innovations and developments are just announcing the start of what could be a new era in archaeological aerial reconnaissance.

Bibliography

Beck, A. 2007. Archaeological site detection: the importance of contrast. In S.n. *Proceedings of the 2007 Annual Conference of the Remote Sensing and Photogrammetry Society* (RSPSoc2007). Newcastle upon Tyne.

Blackburn, G. 2006. Hyperspectral remote sensing of plant pigments. *Journal of Experimental Botany* 58. 855–867.

Buschmann, C. and Nagel, E. 1993. In Vivo spectroscopy and internal optics of leaves as basis for remote sensing of vegetation. *International Journal of Remote Sensing* 14. 711–722.

Caldwell, M. 1971. Solar UV irradiation and the growth and development of higher plants. In Geise, A. (ed.) *Photophysiology.* 131–177. New York: Academic Press.

Carter, G. 1993. Responses of leaf spectral reflectance to plant stress. *American Journal of Botany* 80. 239–243.

Carter, G. 1994. Ratios of leaf reflectances in narrow wavebands as indicators of plant stress. *International Journal of Remote Sensing* 15. 697–703.

Carter, G. and Estep, L. 2002. General spectral characteristics of leaf reflectance responses to plant stress and their manifestation at the landscape scale. In Muttiah, R. (ed.) *From Laboratory Spectroscopy to Remotely Sensed Spectra of Terrestrial Ecosystems.* 271–293. Dordrecht: Kluwer Academic Publishers.

Carter, G. and Knapp, A. 2001. Leaf optical properties in higher plants: linking spectral characteristics to stress and chlorophyll concentration. *American Journal of Botany* 88. 677–684.

Castrianni, L. 2008. Giacomo Boni: a pioneer of the archaeological aerial photography. In Lasaponara, R. and Masini, N. (eds) *Remote Sensing for Archaeology and Cultural Heritage Management. Proceedings of the 1st International EARSeL Workshop, CNR, Rome.* 55–58. Rome: Aracne.

Chappelle, E., Kim, M. and McMurtrey, J. III. 1992. Ratio analysis of reflectance spectra (RARS): an algorithm for the remote estimation of the concentrations of Chlorophyll A, Chlorophyll B, and carotenoids in soybean leaves. *Remote Sensing of Environment* 39. 239–247.

Colwell, R. 1997. History and place of photographic interpretation. In Philipson, W. (ed.) *Manual of Photographic Interpretation,* 33–47. Bethesda: American Society for Photogrammetry and Remote Sensing.

Crawford, O. 1924. *Air Survey and Archaeology*. Southampton: HMSO Ordnance Survey.

Crawford, O. 1929. Air Photographs of the Middle East: a paper read at the evening meeting of the Society on 18 March 1929. *Geographic Journal* 73. 497–512.

Crawford, O. 1933. Some recent air discoveries. *Antiquity* 7. 290–296.

Crawford, O. and Keiller, A. 1928. *Wessex from the Air*. Oxford: Clarendon Press.

Crawshaw, A. 1995. Oblique aerial photography – aircraft, cameras and films. In Kunow, J. (ed.) *Luftbildarchäologie in Ost- und Mitteleuropa. Internationales Symposium, Kleinmachnow, Land Brandenburg*. 67–76. Potsdam: Verlag Brandenburgisches Landesmuseum für Ur- und Frühgeschichte.

Cronin, J., Rooney, T., Williams, R. Jr., Molineux, C. and Bliamptis, E. 1968. *Ultraviolet radiation and the terrestrial surface – AFCRL-68-0572*. Bedford: Air Force Cambridge Research Laboratories.

Doda, D. and Green, A. 1980. Surface reflectance measurements in the UV from an airborne platform. Part 1. *Applied Optics* 19. 2140–2145.

Doda, D. and Green, A. 1981. Surface reflectance measurements in the UV from an airborne platform. Part 2. *Applied Optics* 20. 636–642.

Doneus, M. and Neubauer, W. 2010. LBI for archaeological prospection and virtual archaeology. *AARGNews* 41. 11.

Dorwin, J. 1967. Iodine staining and ultraviolet photography field techniques. *American Antiquity* 32. 105–107.

Gibson, H. 1978. *Photography by Infrared: Its Principles and Applications*. New York: Wiley.

Gitelson, A. and Merzlyak, M. 1994a. Quantitative estimation of Chlorophyll-a using reflectance spectra: experiments with Autumn Chestnut and Maple leaves. *Journal of Photochemistry and Photobiology. B: Biology* 22. 247–252.

Gitelson, A. and Merzlyak, M. 1994b. Spectral reflectance changes associated with autumn senescence of *Aesculus hippocastanum* L. and *Acer platanoides* L. leaves. Spectral features and relation to chlorophyll estimation. *Journal of Plant Physiology* 143. 286–292.

Gitelson, A. and Merzlyak, M. 1996. Signature analysis of leaf reflectance spectra: algorithm development for remote sensing of chlorophyll. *Journal of Plant Physiology* 148. 494–500.

Gitelson, A., Merzlyak, M. and Lichtenthaler, H. 1996. Detection of Red Edge position and chlorophyll content by reflectance measurements near 700 nm. *Journal of Plant Physiology* 148. 501–508.

Gitelson, A., Kaufman, Y., Stark, R. and Rundquist, D. 2002. Novel algorithms for remote estimation of vegetation fraction. *Remote Sensing of Environment* 80. 76–87.

Gitelson, A., Gritz, Y. and Merzlyak, M. 2003. Relationships between leaf chlorophyll content and spectral reflectance and algorithms for non-destructive chlorophyll assessment in higher plant leaves. *Journal of Plant Physiology* 160. 271–282.

Glässer, C., Waldenburger, H. and Gassert, R. 1989. Geowissenschaftliche Anwendung der terrestrischen Multispektralphotographie. *Hallesches Jahrbuch für Geowissenschaften* 14. 89–106.

Grant, R., Heisler, G., Gao, W. and Jenks, M. 2003. Ultraviolet leaf reflectance of common urban trees and the prediction of reflectance from leaf surface characteristics. *Agricultural and Forest Meteorology* 120. 127–139.

Gruzdev, V., Shilin, B., Ivanov, V. and Surikov, I. 2003. Remote observations in the ultraviolet. *Journal of Optical Technology* 70. 350–353.

Guyot, G. 1990. Optical properties of vegetation canopies. In Steven, M. and Clark, J. (eds) *Applications of Remote Sensing in Agriculture.* 19–43. London: Butterworths.

Hampton, J. 1974. An Experiment in Multispectral Air Photography for Archaeological Research. *The Photogrammetric Record* 8. 37–64.

Hatfield, J., Gitelson, A., Schepers, J. and Walthall, G. 2008. Application of spectral remote sensing for agronomic decisions. *Agronomy Journal* 100, Supplement 3. S-117–S-131.

Lyon, R. and Hubel, P. 2002. Eyeing the camera: into the next century. In S.n. *The Tenth Color Imaging Conference: Color Science and Engineering Systems, Technologies, Applications, Scottsdale, Arizona.* 349–355. Springfield: IS&T – SID.

Myers, V., Heilman, M., Lyon, R., Namken, L., Simonett, D., Thomas, J., Wiegand, C. and Woolley, J. 1970. Soil, water and plant relations. In Committee on Remote Sensing for Agricultural Purposes

(ed.) *Remote Sensing With Special Reference to Agriculture and Forestry.* 253–297. Washington D.C.: National Academy of Sciences.

Myneni, R., Maggion, S. Iaquinta, J. Privette, J., Gobron, N., Pinty, B., Kimes, D., Verstraete, M. and Williams, D. 1995. Optical remote sensing of vegetation: modeling, caveats, and algorithms. *Remote Sensing of Environment* 51. 169–188.

Newhall, B. 1982. *The History of Photography from 1839 to the Present*. New York – Boston: Museum of Modern Art.

Palmer, R. 2007. Seventy-five years v. ninety minutes: implications of the 1996 Bedfordshire vertical aerial survey on our perceptions of clayland archaeology. In Mills, J. and Palmer, R. (eds) *Populating Clay Landscapes.* 88–103. Stroud: Tempus.

Ray, S. 2002. *Applied Photographic Optics. Lenses and Optical Systems for Photography, Film, Video, Electronic and Digital Imaging*. Oxford: Focal Press.

Rees, W. 2001. *Physical Principles of Remote Sensing*. Cambridge: University Press.

Rørslett, B. 2004. All You Ever Wanted to Know About Digital UV and IR Photography, But Could Not Afford to Ask. Available at: http://www.naturfotograf.com/UV_IR_rev00.html (accessed 16 November 2010).

Verhoeven, G. 2008. Imaging the invisible using modified digital still cameras for straightforward and low-cost archaeological near-InfraRed photography. *Journal of Archaeological Science* 35(12). 3087–3100.

Verhoeven, G. 2009. *Beyond Conventional Boundaries. New Technologies, Methodologies, and Procedures for the Benefit of Aerial Archaeological Data Acquisition and Analysis.* Zelzate: Nautilus Academic Books.

Verhoeven, G. 2010. It's all about the format – unleashing the power of RAW aerial photography. *International Journal of Remote Sensing* 31(8). 2009–2042.

Verhoeven, G. 2011. Near-InfraRed aerial crop mark archaeology: from its historical use to current digital implementations. *Journal of Archaeological Method and Theory* 19(1). 132–60.

Verhoeven, G., Doneus, M., Briese, C. and Vermeulen, F. 2012. Mapping by Matching – a computer vision-based approach to fast and accurate georeferencing of archaeological aerial photographs. *Journal of Archaeologiacl Science* 39(7). 2060–70.

Verhoeven, G. and Schmitt, K. 2010. An attempt to push back frontiers – digital near-UltraViolet aerial archaeology. *Journal of Archaeological Science* 37(4). 833–845.

Verhoeven, G., Loenders, J., Vermeulen, F. and Docter, R. 2009a. Helikite Aerial Photography (HAP) – a versatile means of unmanned, radio-controlled, low-altitude aerial archaeology. *Archaeological Prospection* 16(2). 125–138.

Verhoeven, G., Smet, P., Poelman, D. and Vermeulen, f. 2009b. Spectral characterisation of a cdigital still camera's NIR-modification to enhance archaeological observation. *IEEE Transactions on Geoscience and Remote Sensing* 47(10). 3456–3468.

Vizy, K. 1974. Detecting and monitoring oil slicks with aerial photos. *Photogrammetric Engineering* 40. 697–708.

Wilson, D. 1982. *Air Photo Interpretation for Archaeologists.* London: Batsford.